SCIENTIFIC REPORTS

OPEN

SUBJECT AREAS:
STRUCTURAL PROPERTIES
SYNTHESIS AND PROCESSING
CATALYST SYNTHESIS
MICRO-OPTICS

Received
21 August 2013

Accepted
20 November 2013

Published
16 December 2013

Correspondence and requests for materials should be addressed to Z.H.H. (huang118@cugb.edu.cn) or S.W.Z. (s.zhang@exeter.ac.uk)

Fe-catalyzed growth of one-dimensional α-Si_3N_4 nanostructures and their cathodoluminescence properties

Juntong Huang[1,2], Zhaohui Huang[1], Shuai Yi[1], Yan'gai Liu[1], Minghao Fang[1] & Shaowei Zhang[2]

[1]School of Materials Science and Technology, China University of Geosciences (Beijing), Beijing 100083, People's Republic of China, [2]College of Engineering, Mathematics and Physical Sciences, University of Exeter, Exeter EX4 4QF, United Kingdom.

Preparation of nanomaterials with various morphologies and exploiting their novel physical properties are of vital importance in nanoscientific field. Similarly to the III-N compound semiconductors, Si_3N_4 nanostructures also could be potentially used for making optoelectronic devices. In this paper, we report on an improved Fe-catalyzed chemical vapour deposition method for synthesizing ultra-long α-Si_3N_4 nanobelts along with a few nanowires and nanobranches on a carbon felt substrate. The ultra-long α-Si_3N_4 nanobelts grew *via* a combined VLS-base and nanobranches *via* a combined double-stage VLS-base and VS-tip mechanism, as well as nanowires *via* VLS-tip mechanism. The three individual nanostructures showed variant optical properties as revealed by a cathodoluminescence spectroscopy. A single α-Si_3N_4 nanobelt or nanobranch gave a strong UV-blue emission band as well as a broad red emission, whereas a single α-Si_3N_4 nanowire exhibited only a broad UV-blue emission. The results reported would be useful in developing new photoelectric nanodevices with tailorable or tunable properties.

One-dimensional (1D) nanostructures have attracted considerable attention since the discovery of carbon nanotubes in 1991[1–8]. Their unique morphologies as well as excellent properties make them potentially applicable to many important areas, such as nanoelectronics[2], energy conversion and storage[9,10], lasers[11], chemical sensing and catalysis[12], and light/field emission devices[13–15]. Differently from its cylindrical counterparts (e.g., nanowire, nanorod and nanotube), a nanobelt possesses a rectangle-like cross section with a high width-to-thickness ratio, providing the nanodevice with a large operable and workable surface, and potentially exhibiting some novel phonon-electron-photon transport properties[16,17], which is of great benefit for developing new generation high-performance nanodevices.

Silicon nitride (Si_3N_4) is an important wide band gap (5.3 eV) semiconductor, as well as an excellent host material with a high ion doping capability, remarkable thermo-mechanical properties and good oxidation and corrosion resistances[18]. A variety of synthesis methods have been attempted to prepare Si_3N_4 1D nanostructures with various morphologies[19–25], many of which were on the Si_3N_4 nanobelt preparation, e.g., vapour-solid thermal reaction between NH_3 and SiO[23], $FeCl_2$-catalyzed pyrolysis of a polysilazane precursor[21] and $NiCl_2$-catalyzed pyrolysis of amorphous silicon carbonitride precursors[25]. Although these techniques could produce high-yield Si_3N_4 nanobelts, they have several limitations which negatively affect the product quality. For instance, in the case of using the vapour-solid reaction routes, Si_3N_4 grains often coexisted with the desired nanobelt products. And in the case of using the pyrolysis precursor routes, much residual carbon from the pyrolysis process often remained in the final products. These problems increased the difficulties in the separation and/or purification of the desired nanobelts. Considering this, it is necessary to explore an alternative novel route to the preparation of high quality Si_3N_4 nanobelts.

In our recent papers, we reported two improved catalytic-thermal chemical vapour deposition (CVD) routes for the growth of high-quality α-Si_3N_4 nanobelts on a carbon felt only using silicon as the main starting raw material, *i.e.*, deposition of $Ni(NO_3)_2$ on a carbon substrate[26] and directly mixing Ni powders with Si powders[27]. The α-Si_3N_4 nanobelts formed on the carbon felt substrate were separated away from the starting raw materials, avoiding the above-mentioned difficulties in the separation and purification. In addition, considering the critical role of nickel in the formation of α-Si_3N_4 nanobelts, we proposed a new combined catalytic vapour-liquid-solid (VLS) base-growth and vapour-solid (VS) tip-growth mechanisms for the nanobelt growth processes. In this work, cheap iron catalysts were used to replace the expensive nickel catalysts previously used to synthesize α-Si_3N_4 nanobelts, so as to further illustrate the reliability of the catalytic-thermal CVD route and validate the

combined growth mechanism proposed earlier. With this work, we have successfully prepared high-yield α-Si_3N_4 nanobelts along with some α-Si_3N_4 nanowires and nanobranches.

Similarly to the III-N compound semiconductors (such as, AlN, GaN and InN), nanostructured Si_3N_4 also could be potentially applied to make optoelectronic and short wavelength optical devices[28]. Previous studies on the optical properties of Si_3N_4 were primarily focused on nonstochiometric amorphous SiN_x films, although the increasing interest has emerged recently in 1D Si_3N_4 nanostructures such as nanowires[29], nanobelts[23], and nanosaws[25]. The spectra were recorded mainly by the photoluminescence (PL) technique on a pile of nanostructures. However, optical properties of each individual α-Si_3N_4 nanostructure still have not been fully understood. So far, there has been only one relevant paper reporting on optical properties of an individual α-Si_3N_4 nanobelt examined by higher spatial resolution cathodoluminescence (CL) technique[30]. According to classical waveguide theory, waveguides of the nanostructures with different cross sections exhibit different transverse optical (TO) modes[31]. Therefore, it is necessary to characterize their luminescence properties of individual α-Si_3N_4 nanostructures with various morphologies.

In this paper, we present our successive work on the growth of α-Si_3N_4 nanobelts using the proposed catalytic thermal-CVD method by changing the catalyst from Ni to Fe. As-prepared α-Si_3N_4 nanobelt products, and some coexisting α-Si_3N_4 nanowire and nanobranch "by-products" were fully characterized. The catalytic effects of iron on the formation of these α-Si_3N_4 nanostructures were discussed and their corresponding growth mechanisms proposed. Furthermore, the CL technique was employed to examine optical properties of as-synthesized individual α-Si_3N_4 nanobelt, nanowire and nanobranch. The present work would provide a good understanding of the relationships between microstructure and luminescence properties, and the guidance for further tailoring or tuning the optical and electric performance in nanostructured semiconductors.

Results

Synthesis and characterization of 1D α-Si_3N_4 nanostructures. A thick white-colored product layer was visually seen on the most area of the carbon felt after 3 h reaction at 1450°C in N_2 upon using Fe as a catalyst. It was peeled from the carbon substrate and subjected to the characterizations using X-ray diffractometer (XRD) and Fourier transform infrared spectroscopy (FT-IR). A broad hump in the low angle region in the XRD pattern (Fig. 1a) arose from the glass sample holder. All other diffraction peaks could be indexed to the hexagonal α-Si_3N_4 (JCPDS Card no. 41-0360), verifying that the product was pure α-Si_3N_4. The FTIR spectrum (Fig. 1b) shows a broad band in the range of 800–1100 cm^{-1} which arises from the Si-N stretching vibration mode of α-Si_3N_4[32]. Moreover, several other absorption peaks around 370–700 cm^{-1} also correspond to the α-Si_3N_4 crystalline structure[33]. Compared to those of the bulk α-Si_3N_4[32], the absorption peaks at 1081 cm^{-1}, 1023 cm^{-1}, 977 cm^{-1} and 863 cm^{-1} here show a blue shift, which should be due to the size- and/or surface-induced quantum effects[34]. These FT-IR results further verified the formation of pure α-Si_3N_4 product.

Microstructures of as-synthesized α-Si_3N_4 products were examined by scanning electron microscopy (SEM). The low-magnification SEM image (Fig. 2a) shows that they exhibited wire-like structures. Most of them were typically a few hundred micrometres long, but some were as long as several millimetres. High-magnification SEM images (Figs. 2b–2f) further reveal that most of them actually possessed a belt-like morphology. Statistical measurements (Fig. 2g) based on SEM images determined that the nanobelts had widths ranging from 300 to 1700 nm and width/thickness ratios from 4 to 10, and presented a unimodal size distribution peaked at ~1000 nm. Each of the nanobelts had a triangular tip (Figs. 2d & 2f, marked by arrow), suggesting a strongly anisotropic growth in the initial stage. Like in the previous case using Ni as a catalyst[27], no particles were observed and no iron catalyst was detected by energy dispersive X-ray spectroscopy (EDS) at tips of the nanobelts. This implies that the growth of the nanobelts should not have been dominated by the well-established VLS-tip mechanism[35]. Furthermore, in addition to the α-Si_3N_4 nanobelts, a few α-Si_3N_4 nanowires as well as nanobranches were seen (Figs. 2h–j). However, differently from the nanobelts, each of the nanowires had a spherical particle at its tip (Fig. 2h), and the branches grew outward from the main stem, exhibiting T-shaped (Fig. 2i) and Y-shaped (Fig. 2j) morphologies, which will be discussed in detail later.

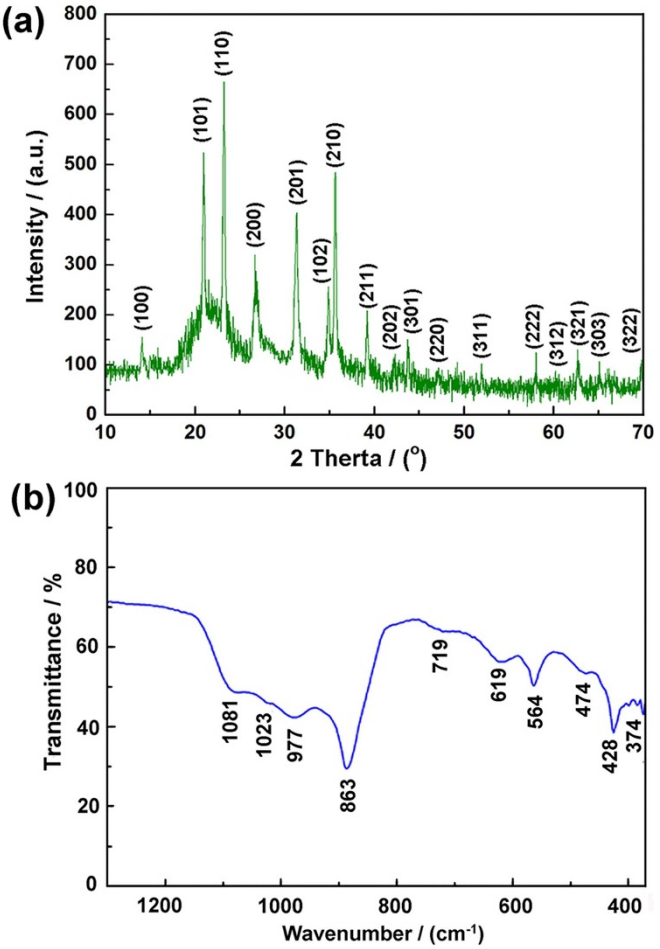

Figure 1 | Phase identification in the as-synthesized product. (a) XRD pattern and (b) FT-IR spectrum of the product detached from the carbon felt.

The three types of α-Si_3N_4 nanostructures obtained were further characterized by a transmission electron microscope (TEM, FEI-Tecnai-G2-F20) and high-resolution TEM (HRTEM). Figure 3 shows the TEM, HRTEM, energy dispersive X-ray spectroscopy (EDS) and selected area electron diffraction (SAED) results of α-Si_3N_4 nanobelts. Typical TEM images (Figs. 3a, b) show that the α-Si_3N_4 nanobelts possessed different widths but a uniform width along the entire length. EDS (Fig. 3c) further identifies that the nanobelts contained Si and N in the atomic ratio of 0.756, very close to the stoichiometric ratio in Si_3N_4 (0.750). Minor Al and O peaks appeared should arise from some contaminations from the corundum balls/jar/tube during the ball milling and/or firing process, whereas Cu signal was from the copper grid sample holder. An individual α-Si_3N_4 nanobelt (Fig. 3b) was characterized entirely by SAED and HRTEM which identified that the nanobelt was a single crystal (Fig. 3d) possessing a perfect crystalline structure with few

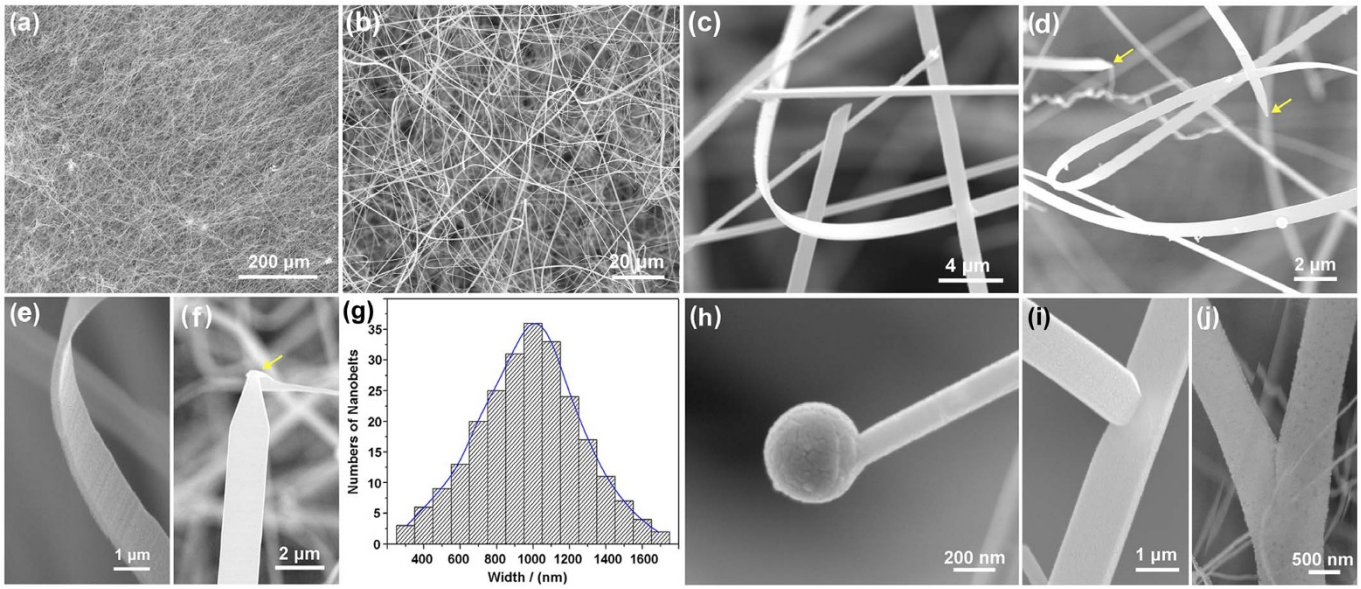

Figure 2 | The SEM images and size distribution of as-synthesized products. (a) Low-magnification and (b) high-magnification SEM images of the products. (c–f) High-magnification SEM images of α-Si_3N_4 nanobelts. (g) Size distribution of as-synthesized α-Si_3N_4 nanobelts. (h) SEM image of a nanowire with a particle attached at the tip. (i–j) SEM images of nanobranches.

defects (Figs. 3e, f). The marked lattice fringes with d-spacing values of 0.56 nm and 0.67 nm in Fig. 3e, f matched with the (001) and (100) planes of α-Si_3N_4. These lattice-fringe values, along with the SAED pattern, suggest that the α-Si_3N_4 nanobelts grew along the [101] direction, and were enclosed by the ±(010) and ±(110) planes. In addition, a few nanobelts were found to be of defect, exhibiting clear stacking faults and misfit dislocations (Figs. 3g, h) which were responsible for the CL behaviour of the α-Si_3N_4 nanobelts, as discussed below.

TEM image (Fig. 4a) shows a straight nanowire with decreasing diameter, and terminated typically with a spherical particle whose diameter was larger than that of the wire itself, and generally appeared darker than the wire. Moreover, EDS (Fig. 4b) reveals that the nanoparticle contained Fe, Si and N elements, along with minor Al and O. HRTEM image (FEI-Tecnai-G2-F20) (Fig. 4c), along with SAED pattern (Fig. 4d), shows more clearly the single-crystalline nature of the nanowire, as well as the gradual decrease in the stacked atomic layers (as shown by arrows) responsible for the taper of the nanowires. The spacing of the lattice fringes parallel to the growth direction was measured to be 0.67 nm, consistent with the d spacing of (100) planes of α-Si_3N_4. The SAED pattern (Fig. 4d) is indexed to the hexagonal crystal structure and indicates the nanowire growth in

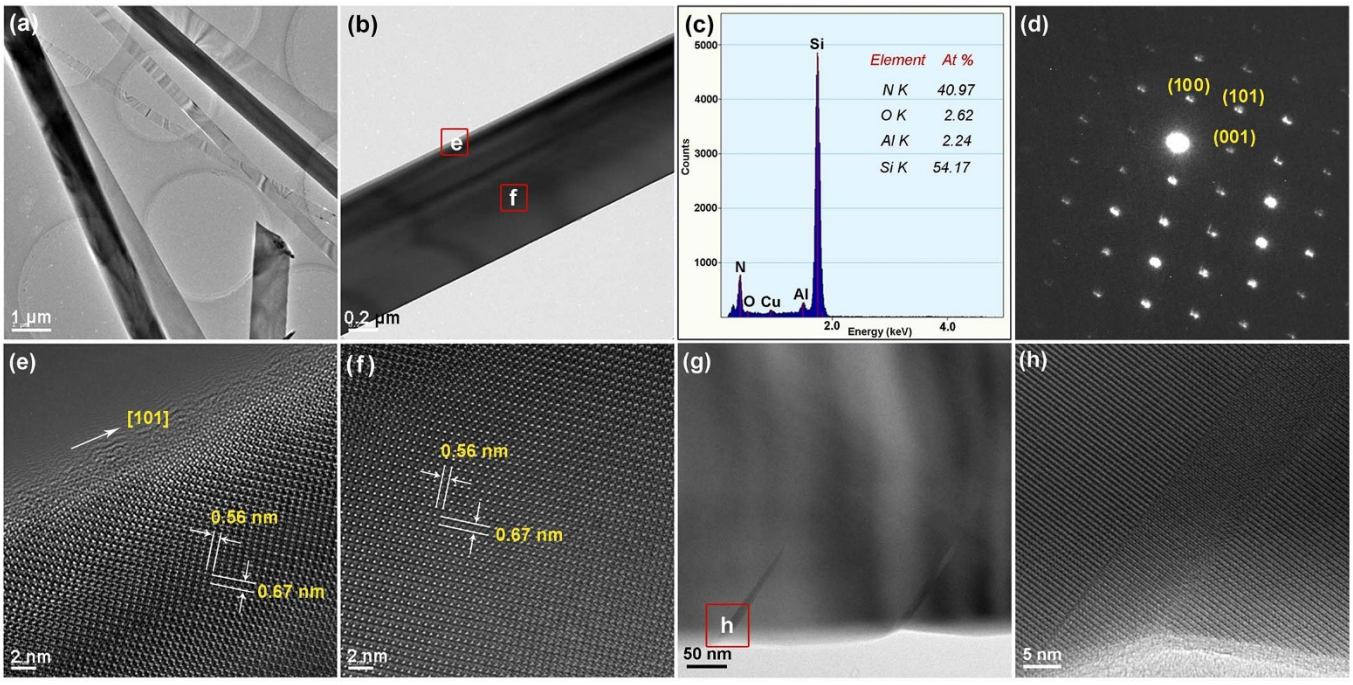

Figure 3 | TEM images of the α-Si_3N_4 nanobelts. (a) A typical low-magnification TEM image of α-Si_3N_4 nanobelts. (b) An individual α-Si_3N_4 nanobelt, (c) corresponding EDX spectrum and (d) SAED pattern of the nanobelt. (e and f) High-resolution TEM images with the α-Si_3N_4 nanobelt shown in Fig. 3b. (g) TEM and (h) HRTEM of an α-Si_3N_4 nanobelt with stacking faults.

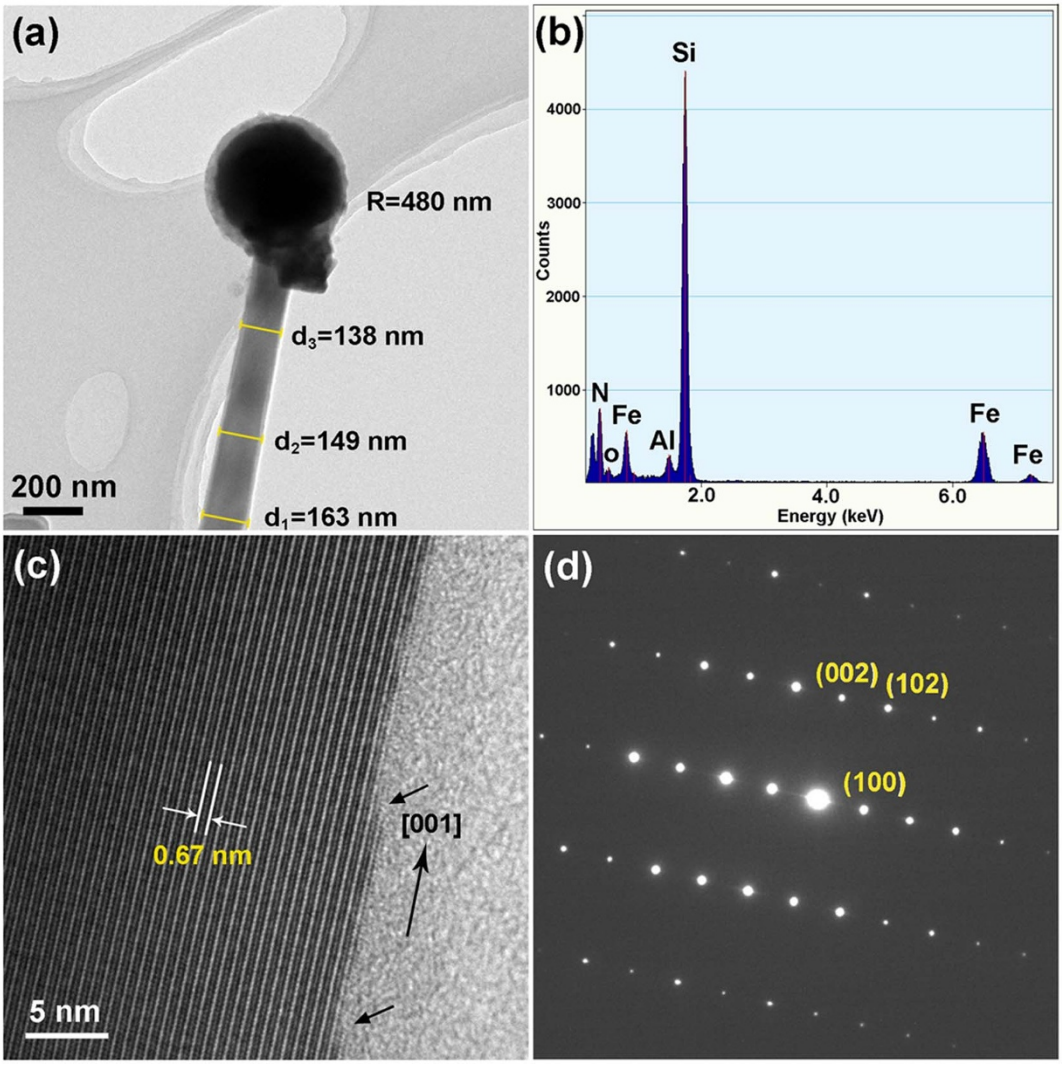

Figure 4 | TEM images of the α-Si_3N_4 nanowires. (a) A typical low-magnification TEM image of an α-Si_3N_4 nanowire, showing a spherical particle on its tip. (b) Corresponding EDX spectrum of the spherical particle. (c) HRTEM image and (d) corresponding SAED pattern of the α-Si_3N_4 nanowire.

the [001] direction. The above results suggested that a VLS-tip growth mechanism might have dominated the formation of the concomitant α-Si_3N_4 nanowires.

Figure 5 presents together TEM (JEOL JEM-2100), HRTEM, EDS and SAED results of α-Si_3N_4 branched nanostructures. The typical Y-shaped (Fig. 5a, b) and T-shaped (Fig. 5c, g) nanobranches were also shown on low-magnification TEM images. Closer observation found that a dark spot was present at the root of a branch (as indicated by a dotted circle in Fig. 5c). EDS analysis (Fig. 5d) reveals that the spot was enrichment of Fe, which as a catalyst should have promoted the nucleation and growth of branches. Figs. 5e–g show several different growth stages of the nanobranches. In the initial growth stage, an enrichment of Fe was formed on the surface of the stem (Fig. 5e), then a small nanorod started to grow from it (Fig. 5f). It grew continuously and finally formed a bigger belt-like branch (Fig. 5g). The SAED patterns recorded from the stem and the branch (insets in Fig. 5g) are almost identical, and can be indexed to the hexagonal structure of α-Si_3N_4. The growth directions of the stem and branch were $[2\bar{1}3]$ and $[\bar{1}\bar{1}3]$, respectively. An HRTEM image of a branch junction (Fig. 5h) reveals that the branch remained epitaxial growth. The SAED patterns along with the HRTEM results suggest that the whole branched structure (stem + branch) was a single crystal.

Effects of Fe on the formation of α-Si_3N_4 nanobelts, nanowires and nanobranches. α-Si_3N_4 nanobelts along with some α-Si_3N_4 nanowires and nanobranches could grow on the carbon felt when iron powders were used with the silicon raw material. In order to illustrate the role of Fe in the formation of these morphologies, in particular, in the formation of nanobelts, we also performed the comparison experiment without using Fe, in which case, fewer and shorter α-Si_3N_4 nanowires, instead of α-Si_3N_4 nanobelts, were generated on the carbon felt (Fig. 6a–b), which twisted and turned in random directions, indicating that the catalyst iron played an important role in the growth process of α-Si_3N_4 nanobelts. To further verify this, we carried out a further test by only using iron powders in an alumina boat covered with a carbon felt and placed in an alumina tubular furnace and fired at 1450°C. Figs. 6c and 6d show SEM images of an original carbon felt and the iron-catalyst-condensed/deposited carbon belt after 1450°C firing, respectively. The catalyst particles formed on the carbon felt were of *ca.* 0.5–1 μm in diameters. Figs. 6e, f show some short α-Si_3N_4 nanobelts which are believed to have just grown on the carbon felt in the initial stage. As shown in Fig. 6e, α-Si_3N_4 nanobelts nucleated and grew in bunches on the carbon felt seemingly in a "weed growth" mode. Their main bodies and tips contained only Si and N, but no Fe. Interestingly, at the root of a short nanobelt (marked by the dotted

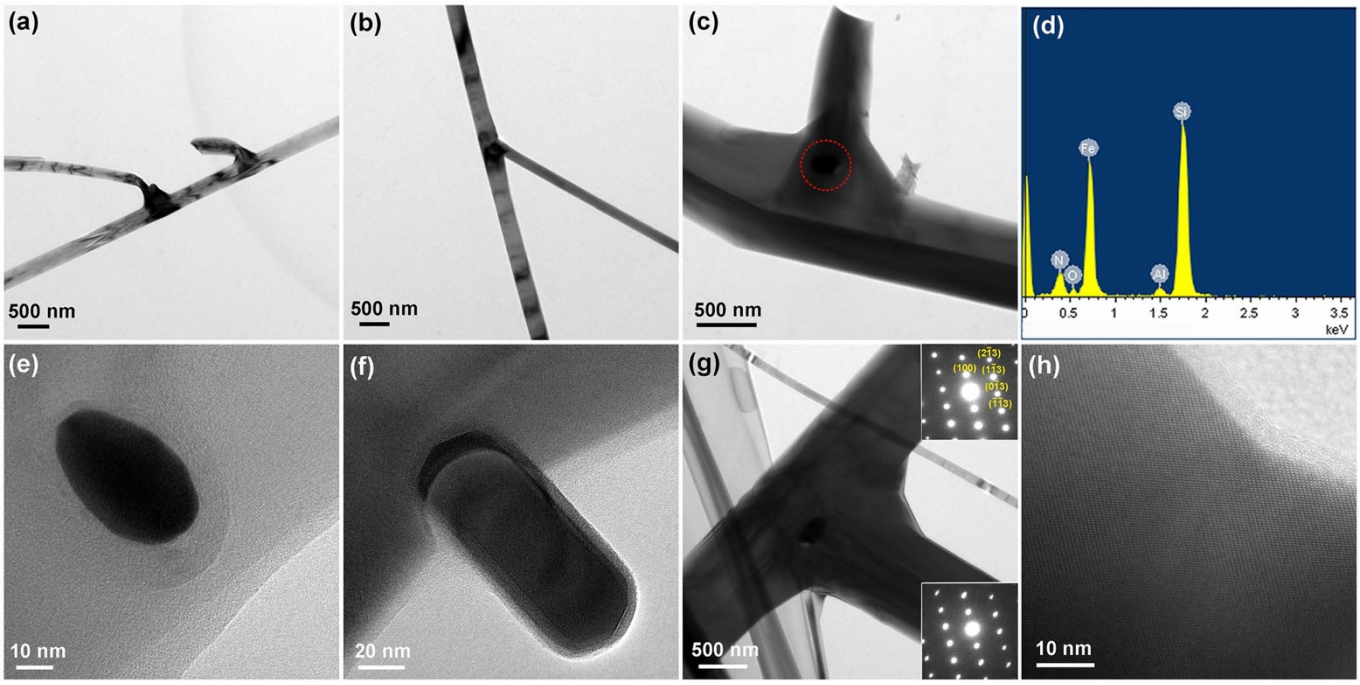

Figure 5 | TEM images of the α-Si_3N_4 nanobranches. (a–b) Typical low-magnification TEM images of α-Si_3N_4 Y-shaped nanobranches. (c) T-shaped nanobranch with a dark spot at the root of a branch, and (d) corresponding EDX spectrum of the dark spot. (e–g) Several growth stages of branched nanostructures. Insets in Fig. 5g were the SAED patterns recorded from the stem and the branch, respectively. (h) An HRTEM image of a branch junction, showing that the branch remained epitaxial.

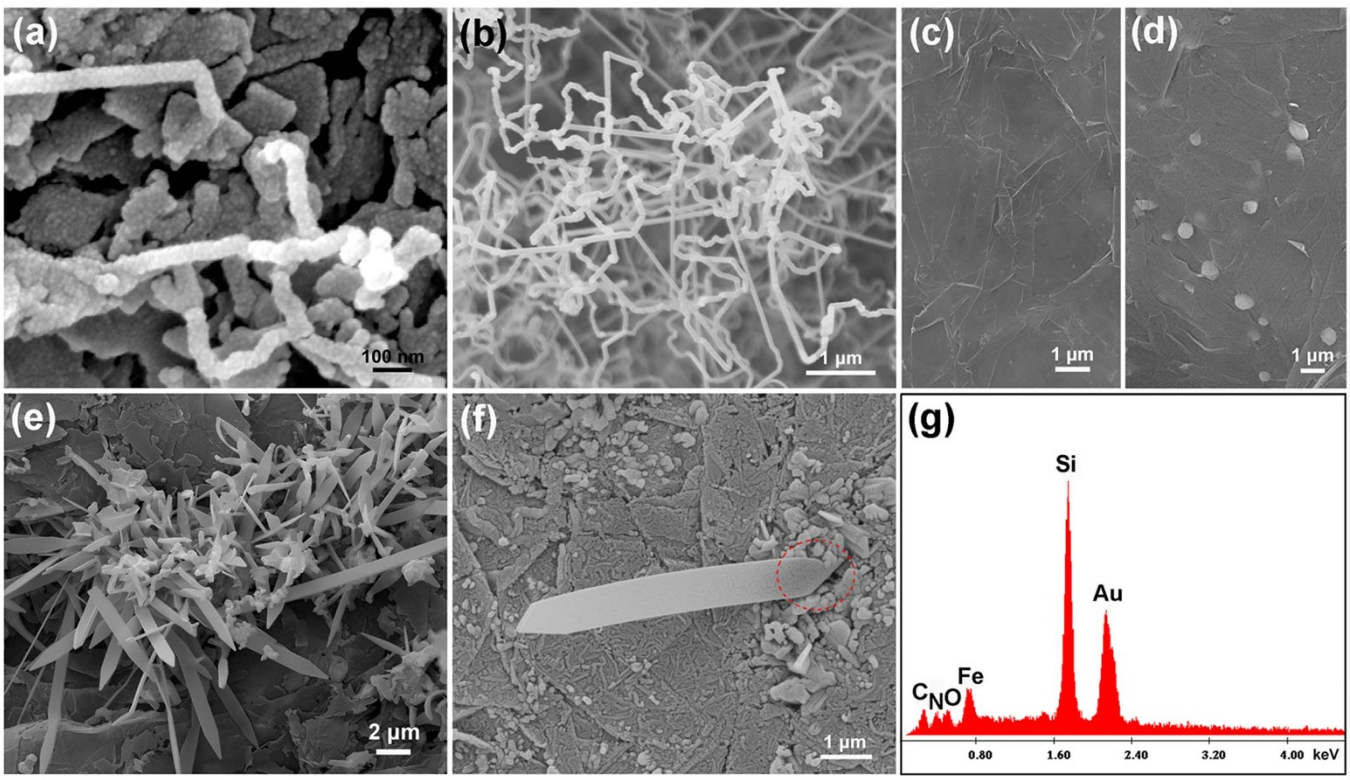

Figure 6 | SEM images and EDS pattern of products. (a–b) SEM images of the as-prepared products in the case of catalyst-absent, showing the nanowire-like structures which twist and turn in random directions. (c) SEM image of an original carbon felt and (d) SEM image of carbon belt with the condensed catalyst iron after being fired at 1450°C. (e and f) SEM images of α-Si_3N_4 nanobelts which had just started to grow from the carbon felt. (g) EDS of the root of nanobelts dotted ring in the Fig. 6f.

ring in Fig. 6f), Fe was detected (Fig. 6g), which is believed to have acted as a "catalyst center" for the nucleation of the nanobelts. Based on this and the results shown in Fig. 6c–d, it can be deduced that although Fe was initially mixed with Si in the alumina boat, it could have been partially transferred to the covering felt via an evaporation and condensation route. Furthermore, based on the comparison with the results on the short and twistable nanowires formed in absence of Fe (Fig. 6a, b), it can be considered that Fe had promoted the formation of the long and straight nanowires and branched nanostructures. The formation mechanisms involved will be discussed in detail later.

Growth mechanisms of 1D α-Si_3N_4 nanostructures. Based on the results described and discussed above, the growth mechanism of as-synthesized α-Si_3N_4 nanobelts as well as nanowires and nanobranches can be schematically illustrated in Fig. 7 and depicted as follows.

VLS-base and VS-tip mechanisms for the α-Si_3N_4 nanobelt formation. In the present work, α-Si_3N_4 nanobelts were successfully synthesized using a catalyst-assisted technique by a thermal CVD method. The growth process of α-Si_3N_4 nanobelts was not completely dominated by the well-established VLS-tip mechanism due to the absence of catalyst-containing particles at tips of the nanobelts. However, like in the case of using nickel as a catalyst reported previously[27], the catalyst iron was found at the root of an nanobelt, which should have promoted the nucleation of α-Si_3N_4 and played a dominant role in the primary formation of its belt-like morphology. Thus, the overall growth mechanism of α-Si_3N_4 nanobelts in this work can be described as follows (schematically illustrated in Fig. 7I): In the initial stage, some iron evaporated from the raw material mixtures in the alumina boat, diffused onto the carbon felt and re-condensed there (Fig. 7Ia, Eqn. 1). Subsequently, Si vapour generated according to Eqn. 2 along with N_2 would diffuse to the Fe particles re-condensed earlier on the carbon felt, forming eutectic Fe–Si–N liquid droplets (Fig. 7Ib, Eqn. 3). When the concentration of Si-N exceeds the saturation level in the Fe-Si-N liquid droplets, the nucleation of α-Si_3N_4 would start, followed by the formation of a prototype nanobelt (Fig. 7Ic, Eqn. 4), which subsequently grew from the droplets (Fig. 7Id). Considering that Fe was only detected in the roots of the nanobelts (Fig. 6f, g) instead of at their tips, the VLS-base growth mechanism rather than the VLS-tip growth mechanism should have governed their growth process. After growing out from the droplets, the nanobelts kept growing along the length direction. In view of the triangular tips of the nanobelts without a nanoparticle, another mechanism, VS mechanism could have contributed to the tip-growth of α-Si_3N_4 nanobelts (Fig. 7Id, e). The growth mechanism depicted here demonstrated once again our previously proposed VLS-base and VS-tip growth mechanism for nanobelts.

$$Fe(s) \xrightarrow{from-raw-materials} Fe(g) \xrightarrow{on-the-carbon-felt} Fe(s) \quad (1)$$

$$Si(s) \rightarrow Si(g) \quad (2)$$

$$Si(g) + N(g) + Fe(s) \rightarrow Fe-Si-N(liquid) \quad (3)$$

$$Si(liquid) + N(liquid) \xrightarrow{Fe-Si-N(liquid)} Si_3N_4(s)_{(\text{nanobelt ``template'' and base-growth})} \quad (4)$$

$$3Si(g) + N(g) \rightarrow \alpha - Si_3N_{4(\text{tip-growth})} \quad (5)$$

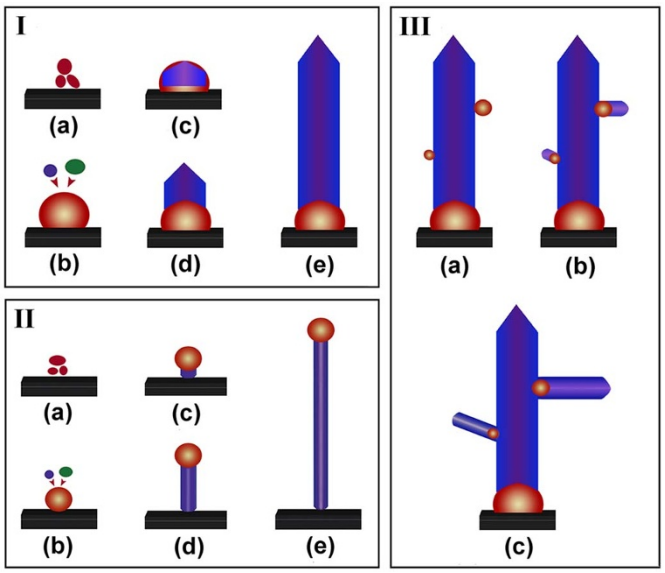

Figure 7 | Simplified growth models of the different α-Si_3N_4 nanostructures. I: For nanobelts (a) The evaporated and re-condensed iron particles on the carbon felt, (b) Formation of Fe-Si-N transition liquid droplet by diffusion of Si and N vapours into iron, (c) Nucleation of α-Si_3N_4 and VLS-base growth of α-Si_3N_4 proto-nanobelt, (d) VS-tip growth and VLS base-growth for α-Si_3N_4 nanobelt and (e) Final long α-Si_3N_4 nanobelt; II: For nanowires (a–b) The process similar to I(a–b), (c) VLS growth for α-Si_3N_4 seed; (d–e) VLS-tip growth for α-Si_3N_4 nanowire; III: For branched nanostructures (a) Catalysts re-condensed on the surface of nanobelts, (b) VLS growth for nanobranches nucleation and growth, (c) Final formed α-Si_3N_4 branched nanostructures.

VLS-tip mechanism for the α-Si_3N_4 nanowires growth. As for the formation of small amount of α-Si_3N_4 nanowires accompanied with the nanobelts, the conventional VLS-tip mechanism is considered to be dominant, since Fe-containing catalyst particles were clearly seen at the growth fronts of the nanowires. In principle, the former several steps (Fig. 7IIa–b) are similar to those for nanobelts (Fig. 7Ia–b, Eqns. 1–3), so they would not be repeated here. Upon oversaturation of Si-N in the Fe-Si-N liquid droplets, α-Si_3N_4 seeds began to precipitate from the supersaturated droplets (Fig. 7IIc, Eqn. 6). As the crystal successively grew, it lifted the liquid catalyst up and eventually grew up to a straight nanowire.

$$Si(liquid) + N(liquid) \xrightarrow{Fe-Si-N(liquid)} Si_3N_4(s)_{(\text{tip-growth})} \quad (6)$$

Double stage VLS-base and VS-tip growth mechanism for the α-Si_3N_4 nanobranched formation. Based on the results shown in Fig. 5 and the relevant discussions above, a double-stage VLS-base and VS-tip growth mechanism is proposed for the α-Si_3N_4 nanobranch growth. Firstly, the first generation (1G) α-Si_3N_4 nanobelts (stems) were formed via a combined VLS base and VS tip growth mechanism, as already stated above (Fig. 7I). Secondly, the catalytic iron particles were deposited onto the surfaces of the stems at random (Fig. 5e, Fig. 7IIIa). Then the second generation (2G) nanobranches would nucleate and grow *via* the aggregation of Si and N vapours into the catalyst followed by a VLS-base growth mechanism (Fig. 5f, Fig. 7IIIb). Finally, those nanobranches continually grew according to some angle directions to form Y-type or T-type branched nanostructures *via* a VS-tip growth mechanism (Fig. 7IIIc).

Cathodoluminescence properties of individual 1D α-Si_3N_4 nanostructures. Room temperature (RT) CL was used to investigate the optical properties of individual α-Si_3N_4 nanowire, nanobelt and nanobranch. To visualize the spatial distribution of the luminescence from them, their SEM images and corresponding CL images were all recorded, as shown in Figs. 8(a, c, e) and 8(b, d, f), respectively. And the CL spectra of these individual nanostructures are shown in Fig. 8g. The light intensity of the emission along the length of all nanostructures almost did not change. However, it was enhanced from an individual α-Si_3N_4 nanowire to nanobelt and to nanobranch, as confirmed by the panchromatic CL images (Fig. 8b, d, f) and CL spectra (Fig. 8g). All of the individual α-Si_3N_4 nanostructures exhibited a strong broad emission from 300 nm to 500 nm located in the ultraviolet(UV)-blue spectral range and a relatively weak broad one from 630 nm to 800 nm located in the red spectral range (Fig. 8g).

Further observation on CL spectra (Fig. 8g) revealed that individual α-Si_3N_4 nanostructures with different shapes exhibited different optical properties. In the CL spectrum of an individual α-Si_3N_4 nanobelt, a strong broad UV-blue emission with two peaks at ~371 nm (3.34 eV) and ~428 nm (2.89 eV) were observed, along with a broad red emission centred at ~733 nm (1.69 eV). In the case of an individual α-Si_3N_4 nanowire, only a broad UV-blue emission centred at ~384 nm (3.22 eV) was present and hardly any red emission was detected, whereas a strongest broad UV-blue emission centred at ~406 nm (3.05 eV) and a red emission centred at ~735 nm (1.68 eV) were observed in the case of an individual nanobranch. The CL properties of α-Si_3N_4 nanostructures here are different from those reported previously by Hu et al.[30] for α-Si_3N_4 nanobelts: an intensive emission from 250 nm to 400 nm, centred at ~305 nm (4.06 eV) and two very weak broad emissions centred at ~540 nm (2.30 eV) and ~735 nm (1.68 eV). They considered that the defect energy levels in Si_3N_4 were responsible for these CL emissions. Robertson[36] classified the defects in Si_3N_4 into four types: Si-Si and N-N bonds, and Si and N dangling bonds. Previous studies suggested that the Si-Si bond formed a bonding σ orbital and an antibonding σ^* orbital, which formed an optical band gap of 4.6 eV[37,38]. The silicon dangling bond formed an energy level at 2.3 eV. The N dangling bonds (N_2^0 centres) formed an energy level at 1.3~1.5 eV, and the N_4^+ defect with an energy level of 3.2 eV[37,38]. The above model can also be used to explain the observed optical behavior of the as-synthesized individual α-Si_3N_4 nanostructures. The UV-blue emissions of α-Si_3N_4 nanobelt, nanowire and nanobranch centred respectively at 3.34 eV, 3.22 eV and 3.05 eV should arise from the recombination between the Si-Si σ^* level and the N_2^0 level or between the N_4^+ and intrinsic valence band edge. Moreover, the red emission centred at 1.69 eV or 1.68 eV should result from the recombination between the N_4^+ and N_2^0 levels.

Discussion

Large amounts of long α-Si_3N_4 nanobelts could grow on the carbon felt upon using catalyst iron in the raw materials, while fewer and shorter twisted α-Si_3N_4 nanowires were generated in the absence of catalyst (Fig. 2, Fig. 6). The eutectic Fe-Si-N liquid droplet is believed to be a "catalyst centre" for the nucleation and growth of the nanobelts (Figs. 6d–f), and have efficiently increased the rate of α-Si_3N_4 deposition to form long nanobelts. According to the previous studies[39–41], the shape of nanostructure products is determined by many factors, such as the growth temperature, supersaturation ratio, the substrate type, surface energies and growth rates. It is believed that the high temperature and/or large supersaturation ratio can facilitate the two-dimensional nucleation, consequently resulting in the formation of belt-like morphology[39]. In our case, Si atoms could combine with N atoms in the eutectic Fe–Si–N liquid droplets to form α-Si_3N_4 with a large supersaturation ratio, which may favour a nucleation and growth of belt-like for α-Si_3N_4.

An interesting thing is that in the case of using Fe as a catalyst, α-Si_3N_4 nanobelts with Fe-containing roots were formed on the carbon felt, whereas a few α-Si_3N_4 nanowires with Fe-containing particles at their tips also presented in the same product samples. The phenomenon was not paid enough attention in our previous work[26,27]. Revealing this could lead to a better understanding for the growth mechanism of α-Si_3N_4 nanobelts. Based on the previous investigations[41], other factors, *e.g.*, the surface energies and growth rates along different crystalline planes and directions, are expected to be also responsible for the nucleation, growth and final morphology of the α-Si_3N_4 product here. The low energy surfaces tend to grow larger and determine the enclosure surfaces of the nanobelts. As a result, the formed molecules tend to diffuse towards the high energy surfaces[39]. Due to the hexagonal structure of Si_3N_4 (*i.e.*, cell parameters $a = b \neq c$), its different planes exhibit different surface energy values ($J \cdot m^{-2}$), such as, $E_{(110)}$ 1.95, $E_{(010)}$ 2.57, $E_{(001)}$ 2.74, $E_{(101)}$ 2.77[42]. Moreover, the differences in growth rates along different crystallographic orientations of Si_3N_4 could be up to 100 times[43,44]. In this study, the ±(010) and ±(110) planes of α-Si_3N_4 have relative low surface energies, so they served as the enclosure surfaces of the final nanobelts. In this case, the incoming Si and N, instead of arriving at these flat low energy surfaces, preferred to diffuse to and then deposit

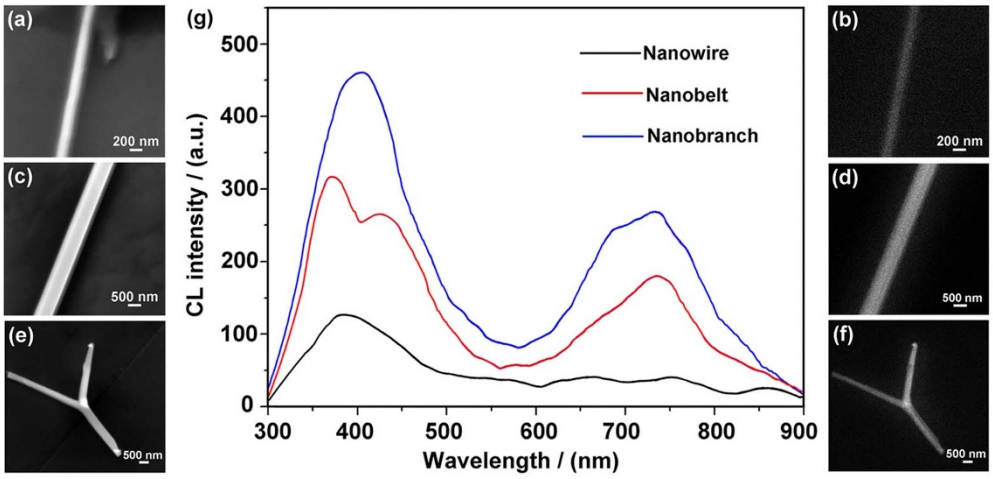

Figure 8 | SEM, CL images and CL spectra of individual α-Si_3N_4 nanostructures. SEM and CL images (a, b) nanowire, (c, d) nanobelt and (e, f) nanobranch. (g) Room-temperature CL spectra of individual α-Si_3N_4 nanowire, nanobelt and nanobranch obtained with a focused electron beam at an accelerating voltage of 20 kV.

on the high energy surface (101) at the length direction [101]. According to the hexagonal structure of Si_3N_4, perpendicular to the [101] direction, its radial direction had the different growth rate, thus leading anisotropic growth in the initial stage, *i.e.*, much more rapid growth along the width direction than that along the thickness direction. As a consequence of the two growth modes at the roots (VLS) and tips (VS) (Fig. 7I), much quicker growth was achieved along the [101] direction than in the thickness or width direction. After the initial short period, the latter would actually stop due to the size-constraining effect of the liquid catalyst droplets (Figs. 2b–d and 6f)), and further growth only occurred along the [101] direction to form ultra-long nanobelts. As for the α-Si_3N_4 nanowires, the [001] was its growth direction (*i.e.*, *c* axial direction) (Fig. 4c) and the (001) plane was a high energy surface. In other words, perpendicular to the *c* axial direction, the radial direction had the same growth rate because of its hexagonal structure, resulting in the formation of nanowires. The fact that α-Si_3N_4 nanobelts with Fe-containing roots instead of tips along with α-Si_3N_4 nanowires with Fe-containing tips were formed on the carbon felt in the same sample products should be related to the bonding between Fe and the growth substrate. Although the exact bonding strength data are unknown, the bonding between Fe and graphitic carbon felt should be strong, considering the good wettability between liquid Fe and graphite (the contact angle $\leq 64^\circ$)[45,46]. The much higher growth rate along the growth direction than that along the width/thickness direction resulted in the formation of triangle morphology at the tip of nanobelt (Fig. 2b&d, Fig. 6f). Such a triangle tip could easily puncture the Fe-Si-N liquid droplet and continue to grow in the initial stage (Fig. 7Ic), leaving the liquid droplet at the roots due to the high pressure (P = F/S). However, the α-Si_3N_4 nanowires had the same growth rate in the radial direction and thus formed a circular plane at their tops, which could push up the liquid droplet from the carbon felt because of the relatively low pressure. The above results and analysis indicated that the use of catalyst Fe should be a necessary but not sufficient condition for the formation of α-Si_3N_4 nanobelts. It would interact with Si and N to form a Fe-Si-N liquid phase which favoured the anisotropic growth of α-Si_3N_4 in the initial stage. Thus, it was more benefit for the formation of α-Si_3N_4 nanobelts than for nanowires viewed from their contents in the products. This work further explained the formation mechanism of the long single crystal α-Si_3N_4 nanobelts and also verified the rationality of the proposed combined catalytic VLS base-growth and VS tip-growth mechanisms although the nanobelt products had a few nanowires and branched nanostructures. Our work also demonstrates the reliability of the technical approach for the synthesis of α-Si_3N_4 nanobelts. This strategy could perhaps be further extended to belt-like growth of III-N semiconductor materials.

In terms of the CL spectra (Fig. 8g), the individual nanobelt exhibited a strong broad UV-blue emission with two peaks centred at ~371 nm and ~428 nm along with a broad red emission centred at ~733 nm, which was different from reported previously (an intensive emission centred at ~305 nm and two very weak broad emissions centred at ~540 nm as well as ~735 nm)[30]. Previous investigations have shown empirically that optical properties of nanomaterials were affected by many factors, such as the intrinsic characteristic, composition, shape and size of nanomaterials as well as structural defects and impurities[47–50]. In this work, the α-Si_3N_4 size (width of ~0.75 μm, Fig. 8c), stacking faults (Figs. 3g, h) and Al-O impurities (Fig. 3c) are considered to be responsible for the different CL emission from the previous report (width of ~7.0 μm). As shown in Fig. 8g, the CL intensity of α-Si_3N_4 nanowire was lower than that of a nanobelt or a nanobranch. In our CL measurements, the penetration depth of the injected electrons could reach hundreds of nanometres, or even several micrometres, under an accelerating voltage of 20 kV. Therefore, the α-Si_3N_4 nanobelt and nanobranch with bigger surface exhibited higher intensity than the nanowire. An even more interesting thing is that an intense UV-blue emission band and a broad red emission exhibited from an α-Si_3N_4 nanobelt or nanobranch, whereas only a broad UV-blue emission from α-Si_3N_4 nanowire. This revealed that individual α-Si_3N_4 nanostructures with different shapes exhibited different optical properties. A similar phenomenon has been observed in several morphologies of CdS nanostructures, which are believed to arise from the surface effect (increased surface-to-volume ratios) and defect concentrations[48,50]. Such reasons could also be used to explain the observed optical behavior of the as-synthesized individual α-Si_3N_4 nanostructures. However, detailed mechanisms on different luminescence properties of the α-Si_3N_4 nanostructures with different shapes are not fully understood and require more systematic investigation.

In summary, we have developed an improved catalytic thermal chemical vapour deposition method for preparing nitride nanobelts. Ultra-long single crystal α-Si_3N_4 nanobelts accompanied with a few nanowires and nanobranches were grown on a carbon felt directly using silicon as the main raw material and Fe as the catalyst. The as-synthesized nanobelts were up to several millimetres long and several hundred nanometers wide, and with width/thickness ratios of 4–10. The shapes of α-Si_3N_4 products were affected by catalyst Fe (supersaturation ratio), surface energies and growth rates. The catalyst efficiently promoted the formation of long and straight α-Si_3N_4 nanostructures. The α-Si_3N_4 nanobelts with Fe-containing roots and triangle tips grew *via* a combined VLS-base and VS-tip mechanism, whereas α-Si_3N_4 nanowires with Fe-containing particles at their tips *via* a VLS-tip mechanism, and α-Si_3N_4 nanobranches *via* a double-stage VLS-base and VS-tip growth mechanisms. The cathodoluminescence technique was used to characterize the luminescence properties of an individual α-Si_3N_4 nanowire, nanobelt and branched nanostructure. Individual α-Si_3N_4 nanostructures with different shapes exhibited different optical properties. An individual α-Si_3N_4 nanowire exhibited only a broad UV-blue emission, whereas an individual α-Si_3N_4 nanobelt and nanobranch exhibited a UV-blue emission as well as a red emission. The work would be useful not only for understanding the fundamental phenomena in low dimensional systems, but also for developing new generation nanodevices with tailorable or tunable photoelectric properties.

Methods

Typical synthesis procedures in this work were similar to those described in our previous paper using Ni as a catalyst[27]. Briefly, a 9 : 1 wt.% mixture of Si powder (99 wt.%, 325 mesh, Aldrich Chemical Company, Inc., UK) and Fe powder (98.5 wt.%, ~2.0 μm, Sagwell Science & Technology CO., LTD, China) in an alumina boat covered with a carbon felt was placed at the center of a long alumina tubular furnace, then heated at 1450°C for 3 h in flow nitrogen (purity 99.999%). Detailed experimental conditions are described elsewhere[27].

The products growing on carbon felt were characterized by X-ray diffraction (XRD, Phillips diffractometer PW1830), Fourier-transform infrared spectrometer (FT-IR, Model Spectrum 2000, Perkin-Elmer, USA), scanning electron microscopy (SEM, FEI-Inspect F, JEOL, Japan) and transmission electron microscopy (TEM, FEI-Tecnai-G2-F20, Philips, Netherlands and JEOL JEM-2100, Japan). The energy dispersive x-ray spectroscopy (EDS) linked with the SEM and the HRTEM, along with selected area electron diffraction (SAED), were employed to assist the phase identification. After the phase and structure examinations, spatially resolved cathodoluminescence (CL) measurements on α-Si_3N_4 nanostructures were carried out. CL spectra from individual α-Si_3N_4 nanobelt, nanowire and nanobranch were collected with a high-resolution CL system at an accelerating voltage of 20 kV and a current of 130 μA by using an ultrahigh vacuum scanning electron microscope (UHV-SEM) equipped with a Gemini electron gun (Omicron, Germany) and a CL detector (Gatan mono 3 plus). The pressure in the specimen chamber was 10^{-3} Pa. All the CL images and spectra were collected at room temperature under identical conditions to ensure convictive comparison.

1. Iijima, S. Helical microtubules of graphitic carbon. *Nature* **345**, 56–58 (1991).
2. Huang, Y. *et al*. Logic gates and computation from assembled nanowire building blocks. *Science* **294**, 1313–1317 (2001).
3. Sardar, K., Deepak, F. L., Govindaraj, A., Seikh, M. M. & Rao, C. N. R. InN nanocrystals, nanowires, and nanotubes. *Small* **1**, 91–94 (2005).
4. Yan, R. X., Gargas, P. & Yang, P. D. Nanowire photonics. *Nat. photonics* **3**, 569–576 (2009).

5. Takai, A., Doi, Y., Yamauchi, Y. & Kuroda, K. Soft-chemical approach of noble metal nanowires templated from mesoporous Silica (SBA-15) through vapor infiltration of a reducing agent. *J. Phys. Chem. C* **114**, 7586–7593 (2010).
6. Yang, S. B. *et al.* Porous iron oxide ribbons grown on graphene for high-performance lithium storage. *Sci. Rep.* **2**, 427; DOI: 10.1038/srep00427 (2012).
7. Bastakoti, B. P., Imura, M., Nemoto, Y. & Yamauchi, Y. Synthesis of MoO_3 nanotubes by thermal mesostructural transition of spherical triblock copolymer micelle templates. *Chem. Comm.* **48**, 12091–12093 (2012).
8. Zhang, Y. J. *et al.* Biopolymer-activated graphitic carbon nitride towards a sustainable photocathode material. *Sci. Rep.* **3**, 2163; DOI: 10.1038/srep02163 (2013).
9. Shi, E. Z. *et al.* Nanobelt-carbon nanotube cross-junction solar cells. *Energy & Environ. Sci.* **5**, 6119–6125 (2012).
10. Luo, J. S. *et al.* Homogeneous photosensitization of complex TiO_2 nanostructures for efficient solar energy conversion. *Sci. Rep.* **2**, 451; DOI: 10.1038/srep00451 (2012).
11. Hu, M.-S. *et al.* Infrared lasing in InN nanobelts. *Appl. Phys. Lett.* **90**, 123109 (2007).
12. Kolmakov, A. & Moskovits, M. Chemical sensing and catalysis by one-dimensional metal-oxide nanostructures. *Annu. Rev. Mater. Res.* **34**, 151–180 (2004).
13. Hu, M.-S. *et al.* Sharp infrared emission from single-crystalline indium nitride nanobelts prepared using guided-stream thermal chemical vapor deposition. *Adv. Funct. Mater.* **16**, 537–541 (2006).
14. Wu, X.-C., Tao, Y.-R. & Gao, Q.-X. Fabrication of TaS_2 nanobelt arrays and their enhanced field-emission. *Chem. Commun.* **40**, 6008–6010 (2009).
15. Mann, D. *et al.* Electrically driven thermal light emission from individual single-walled carbon nanotubes. *Nat Nanotechnol.* **2**, 33–38 (2007).
16. Pan, Z. W., Dai, Z. R. & Wang, Z. L. Nanobelts of semiconducting oxides. *Science* **291**, 1947–1949 (2001).
17. Elfström, N., Karlström, A. E. & Linnros, J. Silicon nanoribbons for electrical detection of biomolecules. *Nano Lett.* **8**, 945–949 (2008).
18. Munakata, F. *et al.* Optical properties of β-Si_3N_4 single crystals grown from a Si melt in N_2. *Appl. Phys. Lett.* **74**, 3498–3500 (1999).
19. Lina, F.-H. *et al.* Study of silicon nitride nanotube synthesis at relative low temperature by thermal-heating chemical-vapor deposition method. *Mater. Chem. Phys.* **93**, 10–15 (2005).
20. Shen, G. Z. *et al.* Systematic investigation of the formation of 1D α-Si_3N_4 nanostructures by using a thermal-decomposition/nitridation process. *Chem. Eur. J.* **12**, 2987–2993 (2006).
21. Yang, W. *et al.* Synthesis of single-crystalline silicon nitride nanobelts via catalyst-assisted pyrolysis of a polysilazane. *J. Am. Ceram. Soc.* **88**, 466–9 (2005).
22. Wang, F., Jin, G. Q. & Guo, X. Y. Formation mechanism of Si_3N_4 nanowires via varbothermal reduction of carbonaceous silica xerogels. *J. Phys. Chem. B* **110**, 14546–9 (2006).
23. Yin, L. W., Bando, Y., Zhu, Y. C. & Li, Y. B. Synthesis, structure, and photoluminescence of very thin and wide alpha silicon nitride (α-Si_3N_4) single-crystalline nanobelts. *Appl. Phys. Lett.* **83**, 3584–3586 (2003).
24. Huo, K. F. *et al.* Synthesis of single-crystalline α-Si_3N_4 nanobelts by extended vapour-liquid-solid growth. *Nanotechnology* **16**, 2282–2287 (2005).
25. Guo, G. F. *et al.* Facile conversion of silicon nitride nanobelts into sandwich-like nanosaws: towards functional nanostructured materials. *Appl. Phys. A* **97**, 729–734 (2009).
26. Huang, J. T. *et al.* Catalyst-assisted synthesis and growth mechanism of ultra-long single crystal α-Si_3N_4 nanobelts with strong violet-blue luminescent properties. *CrystEngComm* **14**, 7301–7305 (2012).
27. Huang, J. T. *et al.* Growth of α-Si_3N_4 nanobelts via Ni-catalyzed thermal chemical vapour deposition and their violet-blue luminescent properties. *CrystEngComm* **15**, 785–790 (2013).
28. Zhang, L. *et al.* Optical properties of single-crystalline α-Si_3N_4 nanobelts. *Appl. Phys. Lett.* **86**, 061908 (2005).
29. Ahmad, M., Zhao, J., Pan, C. F. & Zhu, J. Ordered arrays of high-quality single-crystalline a-Si_3N_4 nanowires: synthesis, properties and applications. *J. Cryst. Growth* **311**, 4486–4490 (2009).
30. Hu, J. Q., Bando, Y., Sekiguchi, T., Xu, F. F. & Zhan, J. H. Two-dimensional extremely thin single-crystalline α-Si_3N_4 microribbons. *Appl. Phys. Lett.* **84**, 804 (2004).
31. Okamoto, K. Fundamentals of Optical Waveguides. (Academic, San Diego, 2000).
32. Wada, N., Solin, S. A., Wong, J. & Prochazka, S. Raman and IR absorption spectroscopic studies on α, β and amorphous Si_3N_4. *J. Non-Cryst. Solids* **43**, 7–15 (1981).
33. Luongo, J. P. Infrared characterization of α- and β-crystalline silicon nitride. *J. Electrochem. Soc.* **130**, 1560–1562 (1983).
34. Ryu, K. H. & Yang, J. M. Microstructure and properties of nanosemicrystalline Si_3N_4 ceramics with doped sintering additives: part I. microstructural characterization of nanosemicrystalline Si_3N_4 powders. *J. Mater. Res.* **13**, 2580–2587 (1998).
35. Wagner, R. & Ellis, W. Vapor-liquid-solid mechanism of single crystal growth. *Appl. Phys. Lett.* **4**, 89–90 (1964).
36. Robertson, J. Electronic structure of silicon nitride. *Philos. Mag. B* **63**, 47–77 (1991).
37. Gao, F. M., Wang, Y. S., Zhang, L. G., Yang, W. W. & An, L. N. Optical properties of heavily Al-doped single-crystal Si_3N_4 nanobelts. *J. Am. Ceram. Soc.* **93**, 1364–1367 (2010).
38. Warren, W. L., Robertson, J. & Kanicki, J. Si and N dangling bond creation in silicon nitride thin films. *Appl. Phys. Lett.* **63**, 2686–2687 (1993).
39. Dai, R. Z., Pan, Z. W. & Wang, Z. L. Novel nanostructures of functional oxides synthesized by thermal evaporation. *Adv. Funct. Mater.* **13**, 9–24 (2003).
40. Hou, W.-C., Chen, L.-Y., Tang, W.-C. & Hong, F. C. N. Control of seed detachment in Au-assisted GaN nanowire growths. *Cryst. Growth Des.* **11**, 990–994 (2011).
41. Hu, M. S. *et al.* Sharp infrared emission from single-crystalline indium nitride nanobelts prepared using guided-stream thermal chemical vapor deposition. *Adv. Funct. Mater.* **16**, 537–541 (2006).
42. Idrobo, J. C., Iddir, H., Öğüt, S., Browning, A. Z. N. D. & Ritchie, R. O. *Ab initio* structural energetics of β-Si_3N_4 surfaces. *Phys. Rev. B* **72**, 241301 (2005).
43. Hwang, C. J. & Tien, T. Y. Microstructural development in silicon nitride ceramics. *Mater. Sci. Forum* **47**, 84–109 (1989).
44. Krämer, M., Hoffmann, M. J. & Petzow, G. Grain growth studies of silicon nitride dispersed in an oxynitride glass. *J. Am. Ceram. Soc.* **76**, 2778–2784 (1993).
45. Zhao, L. Y. & Sahajwalla, V. Interfacial phenomena during wetting of graphite/alumina mixtures by liquid iron. *ISIJ Int.* **43**, 1–6 (2003).
46. Takao, F., Satoru, M. & Yoichi, K. Wetting properties between molten cast iron and graphite. *Reports of the Mie Prefectural Science and Technology Promotion Center Industrial Research Division* **26**, 41–46 (2002).
47. Gautam, U. K. *et al.* Solvothermal synthesis, cathodoluminescence, and field-emission properties of pure and N-doped ZnO nanobullets. *Adv. Funct. Mater.* **19**, 131–140 (2009).
48. Zhang, M. *et al.* Carbon-assisted morphological manipulation of CdS nanostructures and their cathodoluminescence properties. *J. Solid State Chem.* **182**, 3188–3194 (2009).
49. Mettela, G., Boya, R., Singh, D., Kumar, G. V. P. & Kulkarni, G. U. Highly tapered pentagonal bipyramidal Au microcrystals with high index faceted corrugation: Synthesis and optical properties. *Sci. Rep.* **3**, doi:10.1038/srep01793 (2013).
50. Zhai, T. Y. *et al.* Characterization, cathodoluminescence, and field-emission properties of morphology-tunable CdS micro/nanostructures. *Adv. Funct. Mater.* **19**, 2423–2430 (2009).

Acknowledgments

This work was financially supported by National Natural Science Foundation of China (Grant No. 51032007). Y.G. Liu also thanks the Program for New Century Excellent Talents in University (Grant No. NCET-12-0951).

Author contributions

J.T.H., Z.H.H. and S.W.Z. conceived and designed the experiments. J.T.H. and S.Y. carried out the experiments. J.T.H., Y.G.L. and M.H.F. analyzed the data. All authors discussed the results. J.T.H., Z.H.H. and S.W.Z. wrote the paper.

Additional information

Competing financial interests: The authors declare no competing financial interests.

How to cite this article: Huang, J.T. *et al.* Fe-catalyzed growth of one-dimensional α-Si_3N_4 nanostructures and their cathodoluminescence properties. *Sci. Rep.* **3**, 3504; DOI:10.1038/srep03504 (2013).